Optical Engineering 45(5), 053605 (May 2006)

Extended-range Shack-Hartmann wavefront sensor with nonlinear holographic lenslet array

Dmytro V. Podanchuk
Volodymir P. Dan'ko
Myhailo M. Kotov
National Taras Shevchenko University of Kyiv
Radiophysical Department
64, Volodymirska Street
Kyiv, Ukraine, 01033

Jung-Young Son, FELLOW SPIE
Yong-Jin Choi
Han-Yang University
Electronics and Electrical Engineering Department
Whole Imaging Laboratory
Seoul, Korea

Abstract. A nonlinear holographic lenslet array is used to extend the angular dynamic range of a Shack-Hartmann wavefront sensor. The lenslet array has two focal distances defined by the first- and second-order diffracted beams. The second-order beam channel is used for preliminary estimation of the spot position in the first-order beam channel. The sensor has an angular dynamic range twice as large as that of a sensor with single-focus lenslets, while retaining the same accuracy. © *2006 Society of Photo-Optical Instrumentation Engineers.* [DOI: 10.1117/1.2202358]

Subject terms: Shack-Hartmann wavefront sensor; nonlinear holographic lenslet array; coprocessing; higher diffraction orders; dual focus.

Paper 050307 received Apr. 20, 2005; accepted for publication Sep. 30, 2005; published online May 4, 2006.

1 Introduction

Wavefront measurements find wide applications in adaptive optics and metrology.[1,2] The Shack-Hartmann wavefront sensor is often used for these purposes. It is quite simple and convenient for application. The Shack-Hartmann sensor measures the local slope of a wavefront by reconstructing its shape with a special computational procedure.

Basic elements of the Shack-Hartmann wavefront sensor are a lenslet array, and a CCD photodetector located in the focal plane of the lenslets. Every lenslet of the array produces a point image on the photodetector. The shift of each image from its optical axis is directly proportional to the local slope of the wavefront in the corresponding lenslet subaperture. The focal length of the lenslets and the smallest shift of the image that still can be measured with a photodetector determine the angular sensitivity of the sensor. The maximal measurable angle of the wavefront sensor is directly proportional to the size of the subaperture and inversely proportional to the focal length of the lenslets. The traditional method of increasing the maximal measurable value of the wavefront slope consists in reducing the focal length of the lenslet array. But this reduction decreases the angular sensitivity. This problem can be avoided by using a multifocus holographic lenslet array.[3] But recording this type lenslet array is somewhat cumbersome, because it requires two object beam channels with different focal lengths and separate exposure of each channel. Furthermore, aligning the channels to get a desired combination of the focal lengths is difficult.

In this paper, a method of increasing the maximal measurable value of wavefront slope, while maintaining sufficient angular sensitivity, by using a dual-focus nonlinear holographic lenslet array in a Shack-Hartmann wavefront sensor is described.

2 Nonlinear Holographic Lenslet Array

The nonlinear properties of a hologram have been successfully used in holographic interferometry.[4] The nonlinear rewriting of a double-exposure hologram makes the interferometric measurement more sensitive. The ability of a nonlinear hologram to reconstruct the higher-order diffracted beams can be used for the fabrication of a holographic lenslet array (HLA) for a Shack-Hartmann wavefront sensor.

A nonlinear HLA is an array consisting of an absorption hologram recorded on a photosensitive material under nonlinear conditions by interfering the reference plane and objective convergent spherical beams. If the spherical beam is focused at a point behind the hologram with coordinates $(b,0,F)$, then the phase of n' th-order reconstructed beam, $\varphi_n(x,y)$, is represented by the parabolic approximation as[5]

$$\varphi_n(x,y) = \frac{2\pi}{\lambda}\frac{n}{2F}(x^2+y^2-2bx). \tag{1}$$

Hence F is the focal length of the microlens defined by the first-order diffracted beam. For the second-order diffracted beam $(n=2)$, the phase $\varphi_2(x,y)$ becomes two times $\varphi_1(x,y)$. Since the factor $1/2F$ in $\varphi_1(x,y)$ can be written as $1/2(F/2)$ in $\varphi_2(x,y)$, the second-order diffracted beam is focused at a distance $F/2$, i.e., the focal length of the HLA for the second-order beam is $F/2$. Hence a HLA with two spatially separated focal lengths F and $F/2$ is obtained.

The one inherent problem with this nonlinear hologram is that the diffraction efficiency is essentially different for different diffraction orders. But this problem can be eased by changing the operating point on the transmittance-versus-exposure curve of the photomaterial used for recording. The transmittance of the hologram, $t(E_0,\Delta E)$, can be described by Taylor's series about operating point E_0:

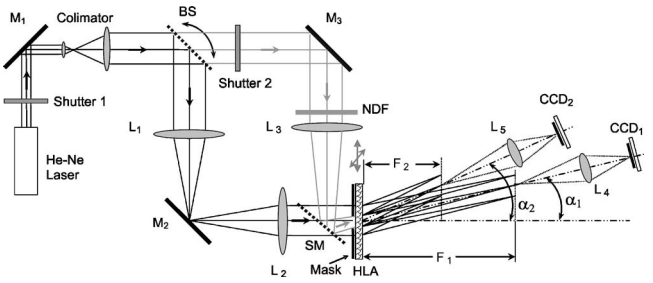

Fig. 1 Experimental setup for recording and investigating nonlinear holographic lenslet array. He-Ne laser, $\lambda=0.6328$ μm; M_1, M_2, M_3: 100% mirrors; BS: beamsplitter; L_1, L_2, L_3, L_4, L_5: lenses; NDF: neutral-density filter; SM: semitransparent mirror; HLA: nonlinear holographic lenslet array; CCD_1, CCD_2: CCD area sensors.

$$t(E_0,\Delta E)=\sum_{n-0}^{\infty} c_n\,\Delta E^n, \tag{2}$$

where ΔE is the modulating term and

$$c_n=\frac{1}{n!}\left.\frac{\partial^n t(E)}{\partial E^n}\right|_{E_0}. \tag{3}$$

The ratio between the diffraction efficiencies of the n' th and first diffraction orders is

$$\eta_n(E)=\left|\frac{c_n}{c_1}\right|=\left|\frac{\partial^n t(E)/\partial E^n}{n!\;\;\partial t(E)/\partial E}\right|_{E_0}. \tag{4}$$

It is quite small on the linear section of exposure characteristic, but an order of magnitude greater on the nonlinear section. Thus, optimal choice of the operating point allows using high diffraction orders (the third or fourth, for example) and optimizing the ratio between the diffraction efficiencies of the operating orders. Hence further expansion of the angular dynamic range of the Shack-Hartmann wavefront sensor will be possible.

A nonlinear HLA has been recorded to work as a dual-focus HLA in a laboratory optical setup as shown in Fig. 1. A laser beam is expanded to a diameter of 10 mm by collimating optics and then divided into two beams by a beamsplitter BS. The beam reflected from BS is focused on the surface of mirror M_2 by lens L_1, and then collimated again by lens L_2 and incident normally on the photoplate as a reference beam. The transmitted beam from BS is reflected 90 deg by mirror M_3, converged by lens L_3, and directed to the photoplate by the semitransparent mirror SM with angle of incidence 9.8 deg. This beam is focused at a distance of 80 mm behind the photoplate. It works as the object beam. A mask with circular aperture located in front of the photoplate confines the incident beams to the diameter of 0.5 mm. A microlens array of 9×7 holographic microlenses with diameter 0.5 mm is recorded with shutter 1 by sequentially moving the holographic photoplate in two orthogonal directions. Nonlinear recording was provided by adjusting the visibility of the interference pattern to nearly 1 and controlling the exposure and developing times of the photoplate (PFG-01 of Slavich, Russia).

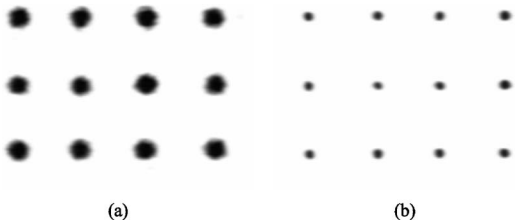

Fig. 2 Part of the spot array image in each focal plane of the nonlinear holographic lenslet array: (a) $F_1=80$ mm, (b) $F_2=40$ mm.

3 Experimental Setup and Data Processing

The photoplate is developed as a nonlinear HLA and is used as a sensing element for the Shack-Hartmann wavefront sensor, which is composed of the same optical setup for recording but without the object beam channel. The channel is shut by shutter 2. The HLA forms two images of a focal spot array (hartmannogram) at distances $F_1=80$ mm and $F_2=40$ mm, respectively. The images of the spot array are shown in Fig. 2.

The optical axis of the HLA is inclined to the normal to the HLA plane at angles of $\alpha_1=9.8$ deg for the first-order diffracted beam and $\alpha_2=19.6$ deg for the second order. The spot array images are imaged by lenses L_4 and L_5 on CCD area sensors CCD_1 and CCD_2, respectively, with demagnification of 1.5. CCD_1 and CCD_2 have 512×582 pixels each. Signals from the CCDs are digitized by corresponding framegrabbers and processed by a computer. The setup allows constructing the sensor with rough (smaller focal distance) and precise (larger focal distance) measurement channels. Images of the focal spot arrays for both focal distances are coprocessed. The shift in a focal spot is defined as the difference between centroids of the spots in the experimentally obtained and reference hartmannograms for each focal length within the boundary of the respective subaperture. The reference hartmannogram of both channels is produced by directing a plane wave normally to the HLA.

The aberration and the noise in the short-focus channel are not substantial, because the channel is used only for preliminary estimation of the spot position in the precise channel. The spot positions in long-focus channel are estimated from the shifts of spots in the x and y directions, Δx_{F_2} and Δy_{F_2}, respectively, measured in the short-focus channel as follows:

$$\tilde{x}_{F_1}=x_{F_1}^{\mathrm{ref}}+\frac{F_1}{F_2}\,\Delta x_{F_2}\quad\text{and}\quad\tilde{y}_{F_1}=y_{F_1}^{\mathrm{ref}}+\frac{F_1}{F_2}\,\Delta y_{F_2}, \tag{5}$$

where $x_{F_1}^{\mathrm{ref}}$ and $y_{F_1}^{\mathrm{ref}}$ are coordinates of corresponding spot in the reference hartmannogram in the long-focus channel.

The position $(\tilde{x}_{F_1},\tilde{y}_{F_1})$ is considered as the center of the subarea in which the precise spot centroid coordinates (x_{F_1},y_{F_1}) are to be determined. Then the shifts of spot center in the x and y directions—Δx_{F_1}, Δy_{F_1}, respectively—in the precise channel can be easily calculated from the reference image. This coprocessing allows increasing the maximal measured angle to the value defined by the short focus while retaining the accuracy defined by the long focus.

For the reconstruction of the wavefront from the calculated local slope values, the modal method[1] is applied. It

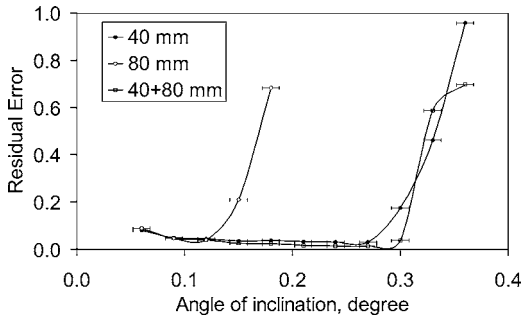

Fig. 3 Residual error of reconstructed tilted wavefronts.

enables us to find expansion coefficients of the wavefront in the basis of characteristic functions (modes). In the method, the phase of the wavefront can be expressed as

$$\Phi(x,y) \approx \Phi_K(x,y) = \sum_{k=1}^{K} a_k g_k(x,y), \tag{6}$$

where a_k are expansion coefficients, and $g_k(x,y)$ basis functions. The functions used are Zernike polynomials.[6] The function $\Phi_k(x,y)$ in Eq. (6) is an approximation of the real wavefront $\Phi(x,y)$ by counting only K modes. In practice, the wave being measured can be described by small number of modes. The quality of the wavefront reconstructed from the experimental data is estimated by the residual error. The error depends on two factors: (1) the number of modes considered in Eq. (6), and (2) the random error of spot position estimation.[7] The finite number of modes leads to projection error, as evident from Eq. (6). The projection error will decrease rapidly to zero when the number of modes reaches an optimum number K_0. The random error results from the measurement errors and random noise. It will slowly increase when the number of modes increases. The residual error of the reconstructed wavefront is represented as

$$\delta^2 = \frac{|\mathbf{u} - \tilde{\mathbf{u}}_1|^2}{|\mathbf{u}|^2}, \tag{7}$$

where $\mathbf{u}$ and $\tilde{\mathbf{u}}_1$ are the vector representations of the measured shift in a spot centroid and the shift of the spot calculated from the reconstructed wavefront, respectively. The wavefront reconstruction procedure with the optimum number of the modes yields the minimal residual error. Its increase indicates growth of the measurement error. This informs us that the angular dynamic range of the sensor is exceeded.

Table 1 Angular dynamic range of the Shack-Hartmann wavefront sensor with nonlinear HLA.

Processing	$\delta\Theta$ (deg)	Θ_{max} (deg)	$D=\Theta_{max}/\delta\Theta$
F_2=40 mm	0.0014	0.27	193
F_1=80 mm	0.0005	0.12	240
Coprocessing	0.0005	0.30	600

4 Results and Discussion

A performance test of the Shack-Hartmann wavefront sensor is carried out by changing the beam incidence angle (i.e., the wavefront tilt) on the HLA by rotating BS. By changing the wavefront tilt from 0 to 0.4 deg with a 0.03 deg step, hartmannograms for the two focal lengths are taken. The first-order Zernike polynomial modes are used for reconstructing the wavefront.

In Fig. 3 the dependence of the residual error on the angle of beam inclination is shown for separate data processing (curves labeled "40 mm" and "80 mm") and coprocessing ("40+80 mm"). The residual error increases in the small-angle range due to the increasing influence of the centroid estimation error. The corresponding dependence of the first-order Zernike coefficient of the reconstructed wavefront on the angle of beam inclination is shown in Fig. 4. The value of the maximal measurable angle Θ_{max} can be estimated from these diagrams. The drastic increase in residual error as shown in Fig. 2 and the sharp decreases in the coefficient value in Fig. 3 indicate that the values are exceeding the maximal measurable angle of the sensor. The angle is specified in Table 1.

The standard deviation of the spot centroid positions, σ, was estimated by an ensemble of 50 realizations of spot array images for each focal distance. Then the smallest shift of the image that still can be measured with a photodetector is defined as 3σ. From this value, the angular sensitivity

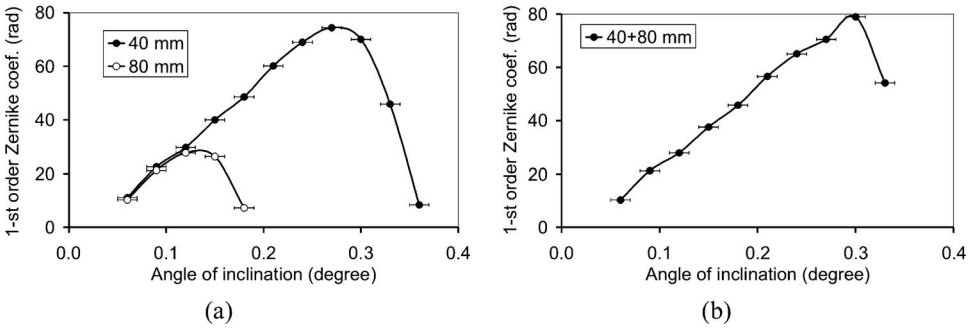

Fig. 4 Reconstructed first-order Zernike coefficients in radians: (a) separate processing of each focal length and (b) coprocessing.

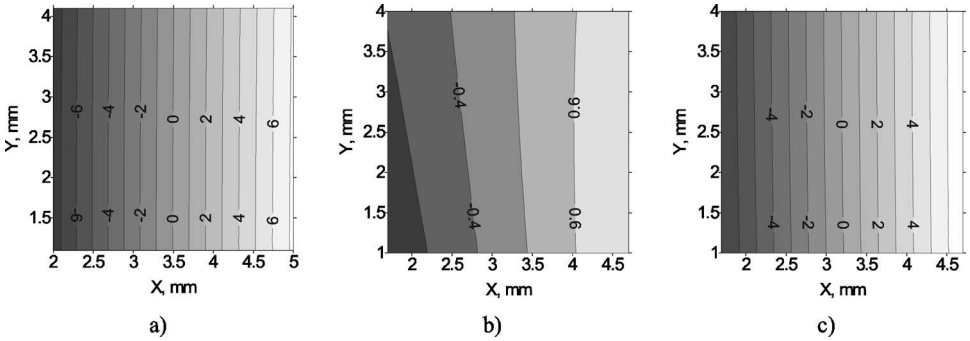

Fig. 5 Contour maps of the reconstructed wavefront for 0.18-deg-tilted wavefronts. (a) $F_2=40$ mm, $Z_1^1=48.70$ rad, peak to valley 14.74λ. Contour curves are drawn with 1λ interval. (b) $F_1=80$ mm, $Z_1^1=7.89$ rad, peak to valley 2.45λ. Contour curves are drawn with 0.5λ interval. (c) Coprocessing, $Z_1^1=45.78$ rad, peak to valley 13.87λ. Contour curves are drawn with 1λ interval.

$\delta\theta$ $(=3\sigma_x/F)$ for each focal length is calculated. The obtained values and calculated angular dynamic range D of the sensor are shown in Table 1. The angular dynamic range of the sensor obtained by coprocessing the two focal distances (80 and 40 mm) of the lenslet array is experimentally shown to be more than twice as large as with 80-mm lenslet array alone, while the accuracy of the sensor is preserved.

In Fig. 5, the result of plane wavefront reconstruction with inclination 0.18 deg is depicted. This angle is within the measurement range of the sensor with focal distance 40 mm. In this case, the contour map of the reconstructed wavefront consists of parallel fringes with spatial frequency corresponding to inclination of 0.18 deg, as shown in Fig. 5(a). For the channel with long focal distance, the reconstructed wavefront is deformed as shown in Fig. 5(b), and hence the incident wavefront cannot be reconstructed. However, the coprocessing of both channels ($F_1=80$ mm and $F_2=40$ mm) provides a good reconstructed wavefront. The contour maps in Figs. 5(a) and 5(c) are practically identical.

The HLA's performance is also measured with the wavefront distorted by second-order aberrations such as defocus and astigmatism. To do this, a complex phase object made by overlapping a concave spherical lens and a convex cylindrical lens is located before the HLA. The overall wavefront local slopes are within the measurement range of the short-focal-distance channel. The average slope is eliminated during the data processing; thus only second-order aberration was reconstructed. The results of reconstructing this wavefront are shown in Fig. 6. The contour maps in Figs. 6(a) and 6(c) are practically identical. The corresponding Zernike coefficients, which represent astigmatism and defocus, are specified in Table 2. The coefficients of the short-focal-distance channel are similar to those in the coprocessing case.

5 Conclusions

It is shown that the nonlinear dual-focus holographic lenslet array can make the angular dynamic range of the Shack-Hartmann sensor more than twice as large as that of the sensor with single-focal lenslets while retaining its accuracy.

The nonlinear multifocus holographic lenslet array is simple to record, and provides precise and identical formation of different measurement channels, and the possibility of adjusting the number of channels and focal-length ratio. But the decreased diffraction efficiency and increased aberrations and noise during the reconstruction lead to decreased accuracy in the spot position measurements in higher diffraction orders. However, they do not affect the accuracy in the precise measurement channel. So the wavefront reconstruction accuracy does not depend on them if coprocessing is applied. For the fabrication of a nonlinear

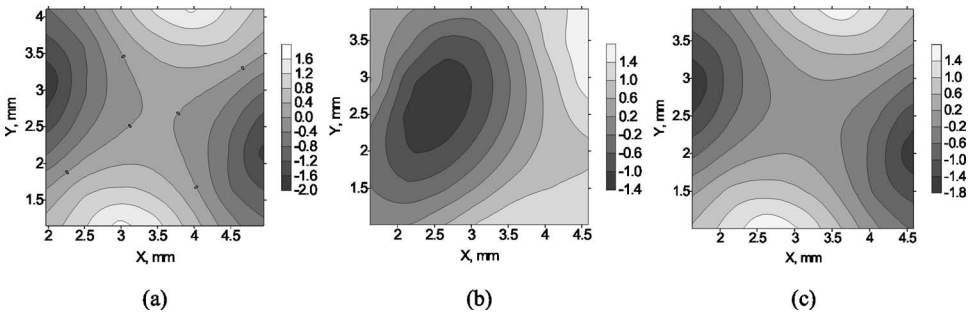

Fig. 6 Contour maps of the distorted wavefronts: (a) $F_2=40$ mm, peak to valley 3.62λ. Contour curves are drawn with 0.4λ interval. (b) $F_1=80$ mm, peak to valley 2.9λ. Contour curves are drawn with 0.4λ interval. (c) Coprocessing, peak to valley 3.48λ. Contour curves are drawn with 0.4λ interval.

Table 2 Zernike coefficients Z_n^m estimated for the wavefront shown in Fig. 6.

Coefficient	Value (rad)			Meaning
	(a)	(b)	(c)	
Z_2^{-2}	−11.04	26.01	−11.16	Astigmatism in ±45-deg direction
Z_2^0	3.50	−13.92	3.50	Defocus
Z_2^2	9.57	5.67	9.69	Astigmatism in horizontal (0-deg) or vertical (90-deg) direction

holographic lenslet array with higher diffraction efficiency a phase hologram can be used. In this case the line of reasoning does not change in principle.

Acknowledgments

The authors thank Dr. V. Kurashov of National Taras Shevchenko University of Kyiv for useful discussions.

References

1. G. Rousset, "Wavefront sensing," in *Adaptive Optics for Astronomy*, D. M. Alloin and J. M. Mariotti, Eds., pp. 116–137, Kluwer Academic (1994).
2. C. R. Forest, M. J. Spenko, Y. Sun, M. McGuirk, M. L. Schattenburg, and A. H. Slocum, "Precision assembly and metrology of x-ray foil optics," *Proc. SPIE* **4851**, 538–548 (2003).
3. J.-Y. Son, D. V. Podanchuk, V. P. Dan'ko, and K.-D. Kwak, "Shack-Hartmann wavefront sensor with holographic memory," *Opt. Eng.* **42**(11), 3389–3398 (2003).
4. A. M. Lyalikov, "Enhancement of the measurement sensitivity in multiple-exposure holographic interferometry," *Opt. Spectrosc.* **93**(1), 136–139 (2002).
5. R. J. Collier, C. B. Burckhardt, and L. H. Lin, *Optical Holography*, student ed., Chap. 12, pp. 337–345, Academic Press, New York (1971).
6. J. Y. Wang and D. E. Silva, "Wave-front interpretation with Zernike polynomials," *Appl. Opt.* **19**, 1510–1518 (1980).
7. M. V. Kapullo, A. V. Kovalenko, and V. N. Kurashov, "Influence of dimensionality of projection space on optical wavefront reconstruction from Hartmann test," *Bull. Univ. Kiev Ser. Phys. Math.* **2**, 264–273 (2003).

Biographies and photographs of authors not available.